Nowcasts of Thunderstorm Initiation and Evolution

JAMES W. WILSON AND CYNTHIA K. MUELLER

National Center for Atmospheric Research*, Boulder, Colorado

ABSTRACT

This paper reports on experimental space-specific 30-min nowcasts of thunderstorm initiation, evolution, and movement. The experiments were conducted near Denver, Colorado, with the purpose of providing weather information for planning purposes to air traffic control managers. The nowcasts were based primarily on Doppler weather radar observations of the clear-air boundary layer, storm reflectivity, storm Doppler velocity structure, and visual observations of clouds. The forecasters found that they could often anticipate thunderstorm initiation by monitoring radar-detected boundary-layer convergence lines together with monitoring visual observations of cloud development in the vicinity of the convergence lines. Nowcast procedures and nowcast results for experiments in 1989 and 1990 are presented. The procedures are based on research experiments and exploratory field tests conducted since 1984. The forecaster results were better than persistence or extrapolation forecasts because of the ability to nowcast storm initiation and dissipation. The results are applicable to weakly forced synoptic situations where storms are typically small and short lived. Forecasters often had difficulty in precisely timing and placing the location of storm initiation. They had even more difficulty in forecasting the evolution of existing storms. Three reasons for these difficulties are believed to be: 1) there are basic deficiencies in our knowledge of the details of storm initiation and evolution, 2) there is a need for detailed observations of boundary-layer thermodynamics and more detailed observations of cumulus cloud location and growth, and 3) many of the forecaster activities were manually intensive and prone to error. Plans for addressing these problems are presented.

1. Introduction

Efficient air traffic flow is dependent on the accurate and precise nowcasts[1] of thunderstorms and related phenomena. The National Center for Atmospheric Research under the sponsorship of the Federal Aviation Agency (FAA) is developing techniques for very short-period nowcasts of thunderstorms. This includes basic research studies and nowcast experiments. Field experiments with these objectives have been conducted in the Denver area every summer since 1985. During 1989 and 1990 spatially specific 30-min nowcasts of thunderstorm[2] initiation, evolution, and movement were made for northeastern Colorado. These nowcasts were primarily based on Doppler radar observations. The radars had sufficient sensitivity to observe the optically clear-air boundary layer. This paper reports on the results of the nowcast experiments and presents an explanation of the nowcast methodology. Thunderstorms in the Denver vicinity are typically single- or multicellular storms (characterized by horizontal scales of 2–20 km) and occur under weakly forced synoptic conditions. They form during the afternoon and evening largely in response to solar heating. Static stabilities are typically near neutral. Extrapolation techniques developed for larger, long-lived, or synoptic-scale forced convection as discussed by Austin (1985), Browning and Collier (1982), and Wilk and Gray (1970) are frequently not effective at this smaller spatial scale. Accurate short-range forecasting in the Denver area requires precise prediction of storm initiation and evolution.

Most thunderstorm initiation nowcasts involve the monitoring of boundary-layer convergence zones (boundaries). Purdom (1973, 1982) was among the first to show the great importance of boundary-layer convergence lines in initiating thunderstorms. These boundaries were frequently visible as lines of cumulus on satellite imagery. A well-known example of a convergence line that is often associated with the initiation of thunderstorms is the "dry line" that forms in west Texas and Oklahoma (Schaefer 1986). Wilson and Carbone (1984) proposed the use of sensitive Doppler radars to monitor boundaries even in the absence of clouds. Carbone et al. (1990) describe the initiation of

---

[1] For the purpose of this paper, nowcast refers to a 0–3-hour forecast that includes extrapolation, evolution, and initiation of weather events.

[2] For the purpose of this paper, thunderstorms are defined as radar precipitation echo with radar reflectivity factors > 30 dBZ.

Corresponding author address: Cynthia K. Mueller, NCAR, P.O. Box 3000, Boulder, CO 80307-3000.

a Kansas squall line by propagating convergence lines observed on radar. Wilson and Schreiber (1986) showed that at least 80% of the thunderstorms in the Denver area formed along radar-detected boundaries. They defined a boundary as "a thin line of enhanced reflectivity and/or a line of apparent convergent flow in Doppler velocity with dimensions of ~1–3 km wide, >10 km long and present for a minimum of 15 min." Boundaries include density currents (Mueller and Carbone 1987), synoptic-scale fronts, topographically induced circulations (Smolarkiewicz and Clark 1985; Szoke et al. 1984; Schreiber-Abshire and Rodi 1991), and differential heating-induced circulations (Pielke and Segal 1986).

A preliminary nowcast experiment based on Doppler radar was conducted in 1988 (Mueller and Wilson 1989). Probability nowcasts of radar reflectivity > 30 dBZ were issued for a 15-min to 3-hr period for two 10-km circles. Figure 1 shows the probability nowcasts versus percent observed for 15-min intervals during the first hour, 30-min intervals during the second hour, and a 60-min interval for the third hour. Figure 1 shows the probability nowcasts were unbiased and reliable although the results are somewhat "noisy" due to small sample sizes. Analyses of these nowcasts using signal detection theory also indicate the forecaster had statistical skill (Harvey et al. 1992). Mueller and Wilson (1989) and Wilson and Mueller (1991) report that these nowcasts based on sensitive Doppler radars were more accurate than persistence or linear extrapolation techniques. A similar experiment conducted in tropical northern Australia (Keenan et al. 1992) showed similar results. Traditionally it has been very difficult to improve on persistence and linear extrapolation techniques during the first-hour forecast period (Tsonis and Austin 1981; Entrekin et al. 1969; Doswell 1986).

While monitoring boundaries is essential for forecasting the general location of new storms, it is not sufficient for determining precisely when and where storms will form. Small-scale spatial (a few kilometers) and temporal (tens of minutes) differences in temperature, moisture, and winds appear to at least partially determine the precise timing and position of new storms (Mueller et al. 1993).

The nowcasts reported here were made throughout an 8000-km^2 region (Fig. 2) by drawing irregular polygons surrounding the areas (median size 200 km^2) where thunderstorms were expected in 30 min. These nowcasts were displayed on video screens in the aircraft control tower at Denver's Stapleton Airport and the Aviation Central Weather Service Unit in Longmont, Colorado. Nowcasts were based primarily on Doppler radar–detected boundaries, precipitation echoes, and visual locations of cloud development. The nowcast methodology reported here and utilized during these nowcast experiments has been used by the Cooperative Program for Operational Meteorology, Education and Training (COMET) to prepare a computer-based
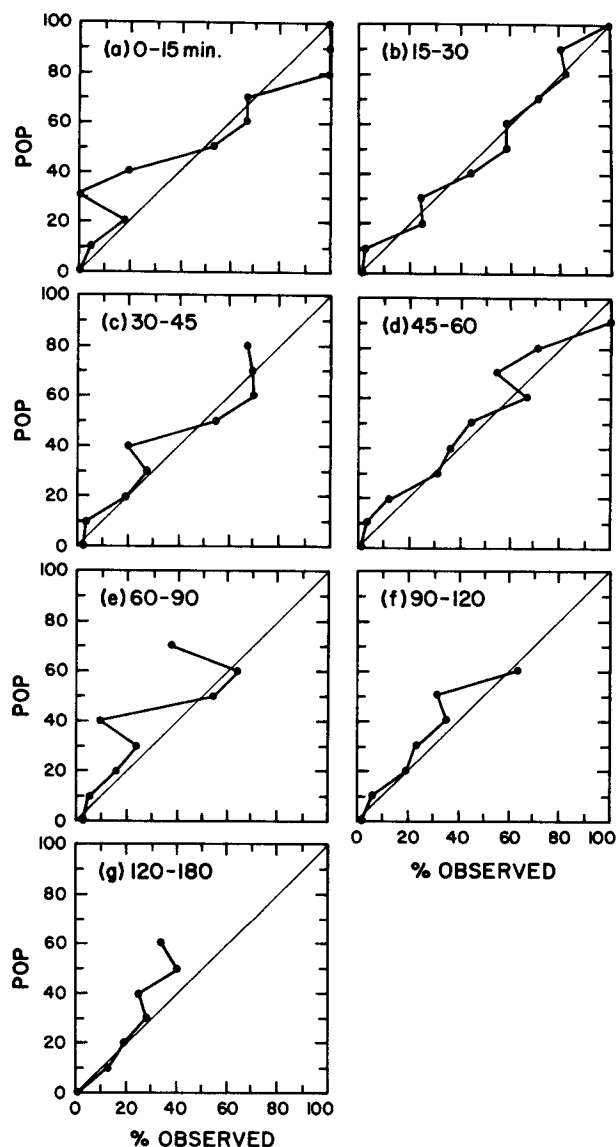

FIG. 1. 1988 results of probability of precipitation (POP) forecasts versus percent of observed precipitation for each of seven forecast intervals (time period indicated in upper-left corner). The forecast area was for a 10-km radius circle centered on Stapleton Airport. Precipitation was defined as the presence of a radar precipitation echo >30 dBZ at 1-km height. If the probability forecasts were precisely calibrated they would fall along the 45° solid line (after Mueller and Wilson 1989).

learning module for the National Weather Service (NWS), the Air Weather Service (AWS), the Naval Oceanography Command (NOC), and the U.S. Army Atmospheric Sciences Division.

Section 2 describes the data, displays, and analysis tools used in the nowcast experiments. Section 3 provides background information on the utility of Doppler radar to detect convergence lines. Section 4 documents the nowcast guidelines and section 5 presents the results
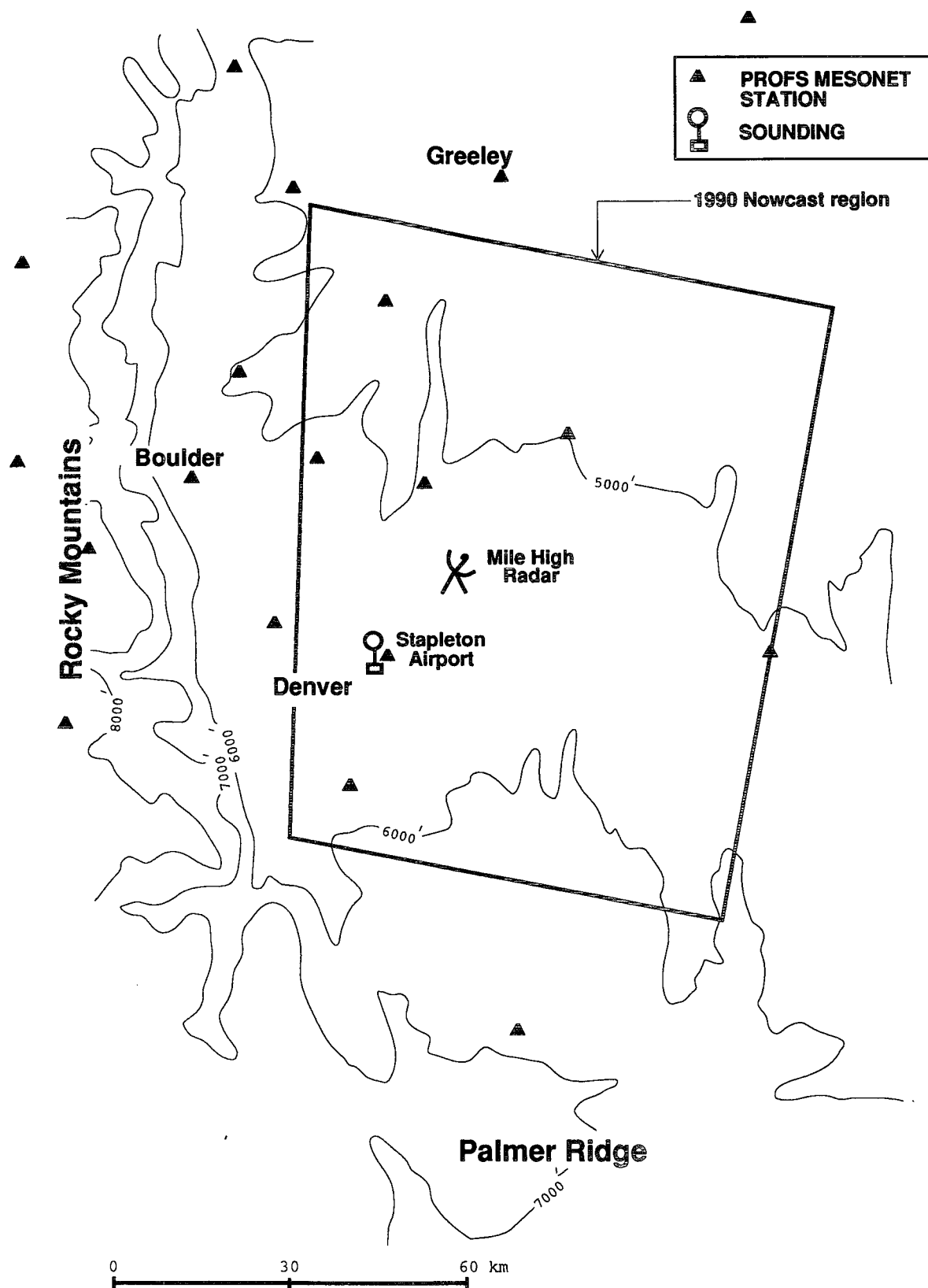
FIG. 2. Location of MHR, PROFS mesonet stations, CLASS sounding, and nowcast region for the 1990 nowcast experiment. The nowcast region for 1989 was the same as 1990 except it did not extend quite as far to the west. Elevation contours are shown in feet above sea level.

of the nowcasts. Section 6 describes plans for future thunderstorm nowcasting efforts.

2. Data, displays, and analysis tools

Figure 2 shows the location of the observation facilities and forecast regions for these nowcasting experiments. Special sensors available to the project were a Doppler radar, one CLASS (Cross-Chain Loran Atmospheric Sounding System) upper-air sounding system (Lauritsen et al. 1987), and the Program for Regional Observing and Forecasting Services (PROFS) mesonetwork (Pratte and Clark 1983). The radar was the NCAR 10-cm wavelength Mile High Radar (MHR) (Pratte et al. 1991). This radar is similar in basic capabilities to the WSR-88D (Alberty et al. 1991). Throughout the paper, examples of radar data will be shown from research radars also of similar sensitivity. These are the NCAR CP-2 Doppler radar (Keeler et al. 1989), NCAR CP-3 Doppler radar (Keeler et al. 1991), and the Lincoln Laboratory FL-2 Doppler radar

(Evans and Turnbull 1985). CLASS soundings were routinely taken from Stapleton Airport at 1700 UTC (1100 MDT). During 1990, additional soundings were occasionally taken by a mobile CLASS. The utility of the PROFS mesonet was limited by the uneven and rather large station spacing (10–75 km) and the moisture measurements were frequently unreliable during this time period.

The data, computer programs, and displays that were available to the forecasters are shown and described in Fig. 3. An interactive workstation developed by PROFS and called Denver Advanced Weather Interactive Processing System (AWIPS) Risk Reduction and Requirements Evaluation (DARRRE) (Dunn 1990) was used to examine the synoptic-scale features and their possible effect on the afternoon weather. Satellite, wind profiler, and mesonet data were also available on this workstation. CLASS sounding data were received at the forecast center via a phone line and later a radio link. Analyses and displays were done using an interactive program developed at NCAR called SUDS (System for User-editing and Display of Soundings).
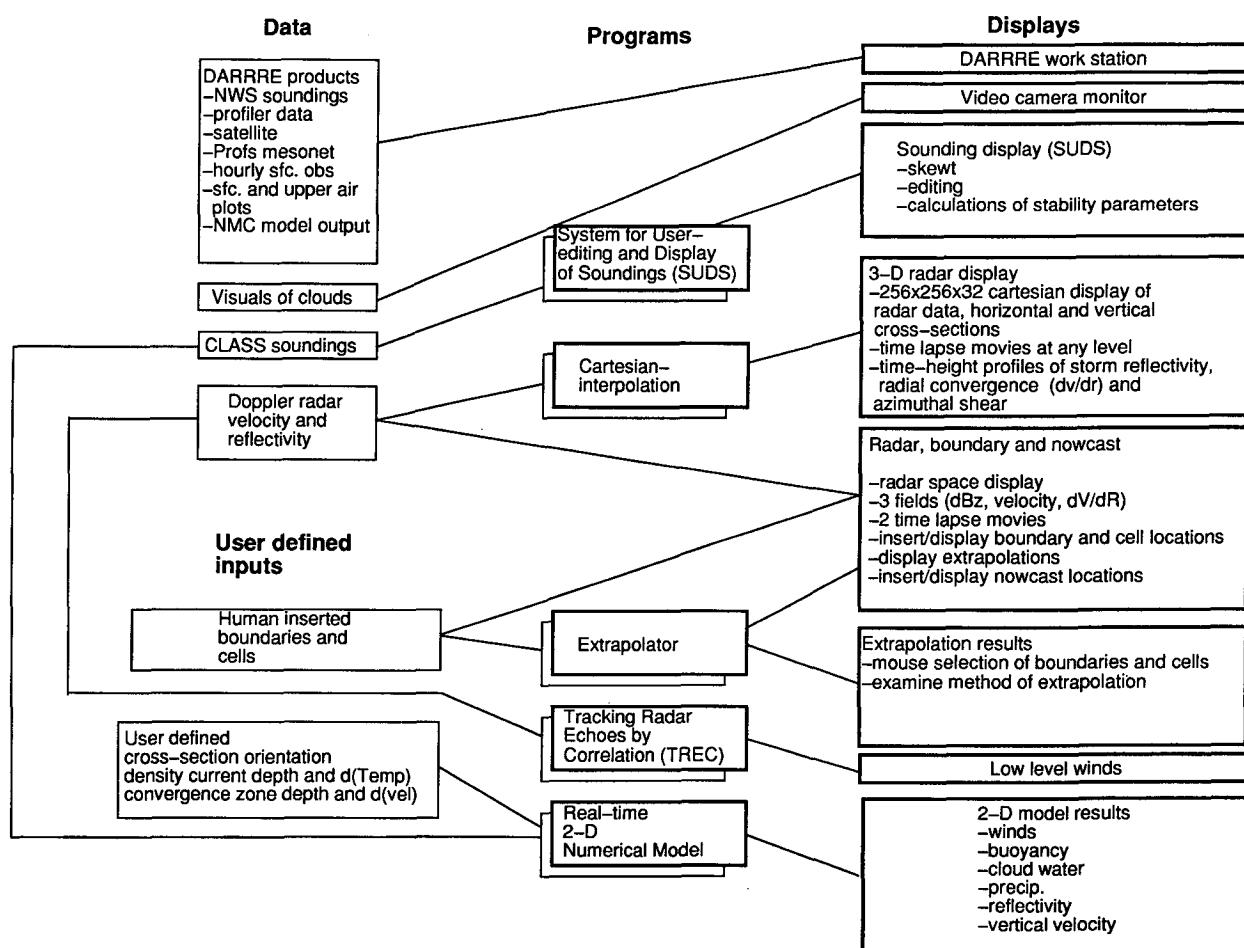

FIG. 3. Diagram of the data, computer programs, and displays available during the 1989 and 1990 nowcast experiments. See text for additional discussion.

Several state-of-the-art color radar displays were available during this period. Some of these displays have been described by Lutz et al. (1989) and Barron et al. (1986). As a minimum, the forecaster had the ability to display in real time, time lapse images of radar reflectivity and Doppler velocity on radar-scanned surfaces. Extrapolation of storms was based on manually entered cell boundaries and cell center points. The cell locations were drawn on the radar images by the forecaster. The cells were linearly extrapolated by the computer, based on past motion, to their expected locations at the time of the next forecast. The forecaster would use the radar displays to identify and monitor boundaries. The boundaries would be drawn on the display and extrapolated along with the cells to the next forecast time.

Visual cloud observations were made by the forecasters using a roof-mounted video camera located on a building in Boulder (see Fig. 2). This meant the forecaster needed to monitor clouds to a distance of 120 km. This is generally possible in the visually clear air of Colorado, but not practical in many other regions. This issue is discussed more extensively in section 6.

3. Radar detection of convergence lines

Sensitive Doppler radars are able to detect boundary-layer convergence lines and horizontal-roll convection in optically clear air (air masses free from precipitation or even clouds) during the warm season (Wilson et al. 1980; Wilson and Schreiber 1986; Christian and Wakimoto 1989). The authors have been involved in numerous field programs in many regions of the United States and northern Australia (Keenan et al. 1991) and have routinely observed the radar detection of convergence lines during warm, mixed boundary-layer conditions. "Clear-air" radar echoes can be attributed to particulate scattering from insects and birds or from Bragg scattering associated with strong gradients in index of refraction caused by moisture and temperature discontinuities (Hardy et al. 1966; Battan 1973; Doviak and Zrnic 1984; Vaughn 1985; Mueller and Larkin 1985; Wilson and Schreiber 1986). Dual polarization and dual wavelength measurements from the NCAR CP2 (Keeler et al. 1989) radar indicate that the scattering mechanism below the boundary layer inversion is primarily from insects (Knight and Miller 1992). Achtemeier (1991) has demonstrated that the enhanced reflectivity in convergence lines results from a concentration of insects. The number increases as a result of the insects resisting the updrafts carrying them to colder heights. They either fold their wings and fall out or fly downward against the updrafts. Thus in convergent updraft regions there will be a net increase in insects since more are coming into the region than are being advected out the top (i.e., the mass continuity equation does not hold for insects).
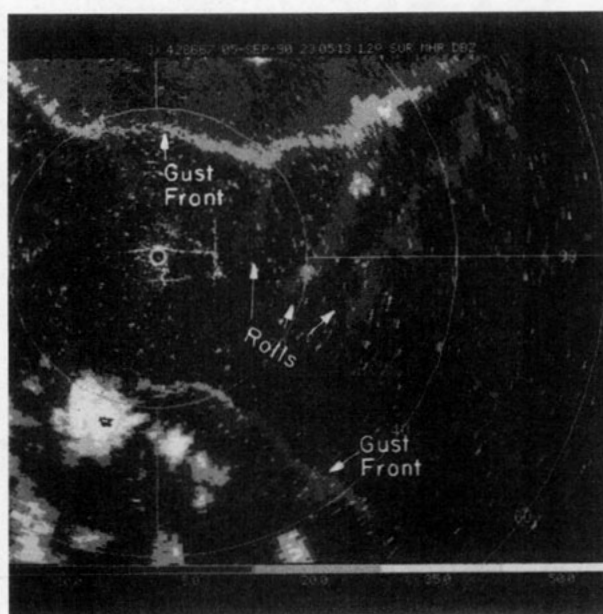
Figure 4 is an example of a radar display from MHR

FIG. 4. Radar reflectivity factor display showing clear-air enhanced thin-line echoes associated with convective horizontal rolls and two gust fronts. The data were collected from the NCAR MHR on 5 September 1990 at 2305 UTC. Reflectivity factors in dBZ are given by the scale at the bottom. The antenna elevation angle is 1.2°. Range marks are at 20-km intervals. This same case is used later in Fig. 11.

during 1990 showing clear-air convergent-line echoes associated with horizontal-roll convection, and two gust fronts. The maximum reflectivity factor in the horizontal rolls is about 10 dBZ and 20–25 dBZ in the gust fronts. Satellite imagery (not shown) show lines of cumulus associated with all three features. Dual Doppler analysis by the authors on similar clear-air echoes (not shown) clearly show the enhanced clear-air reflectivity regions are dominated by updrafts.[3] The "thin line" echo regions associated with the rolls are actually the convergent regions between opposing rotating rolls (Christian and Wakimoto 1989).
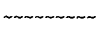
In Figs. 7–10, convergence lines are entered manually on the figures rather than showing the actual thin-line echoes (as in Fig. 4) or Doppler velocity convergence signatures on which these lines are based. This is done to minimize the number of figures and eliminate the need for color figures.

4. Nowcasting guidelines

Based on the 1988 nowcasting experiment (Mueller and Wilson 1989), the results of Wilson and Schreiber (1986), and Mueller et al. (1993) a nowcast meth-

---

[3] Dual Doppler techniques derive vertical air motions in these cases by computing convergence from the synthesized horizontal winds and then integrating the mass continuity equation from the ground upward.

Legend

```
——▶  Quantitative        [shaded box]  forecast region         ⬭ ————  thunderstorm and boundaries present
                                                                         at forecast time
— —  Subjective          ~~~~~~~~~  cumulus clouds              ⬭ — — —  extrapolated positions of thunderstorm and
                                                                         boundaries
                                                                ◯  <30 dBZ cell    ⬭  extrapolated <30 dBZ cell
```
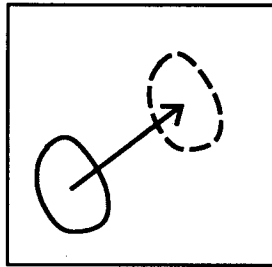
A) Cell Extrapolation

A1) No change

A2) Dissipation

A3) Growth
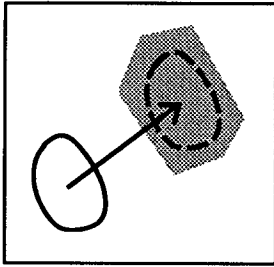
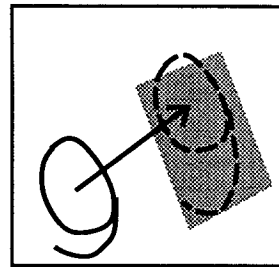Issue forecast for thunderstorm if;

— — Thunderstorm is large
(~ 10 Km diameter)

Locate box based on following;

——▶ Use extrapolated position
and allow for errors in
extrapolation

Issue forecast for dissipation if;

— — Thunderstorm is small
particularly if Doppler
velocity indicates surface
divergence

— — Thunderstorm is moving off
the mountains and there is
no nearby boundary

Issue forecast for growth if;

— — Doppler velocity indicates
strong surface convergence

— — Mesonet and sounding suggest
negative lifted index

— — Thunderstorm moving from
mountains to plains along
a boundary

— — Thunderstorms expected to
merge

Locate box based on following;

— — Use extrapolated position
and allow for growth on
inflow side and dissipation
on down wind side

B) Thunderstorm initiation by boundary

B1) Moving

15 km   / cloud
          / streets

B2) Colliding

10 km

B3) Stationary

10 km
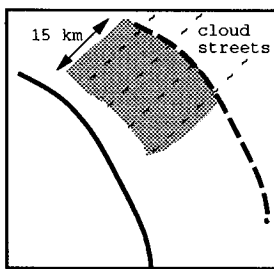
Issue forecast for thunderstorms if;

——▶ There is new cell growth aloft associated
with a boundary (10-20 dBZ at 4-8 km agl)

or if;

——▶ Moving or colliding boundary extrapolated into
cumulus field (generally associated with
horizontal rolls).

or if the two following criteria are meet;

_ _ There is cumulus congestus or towering cumulus
along boundary

_ _ Surface mesonet and morning sounding suggest
negative MLI (surface mixing ratio is critical)
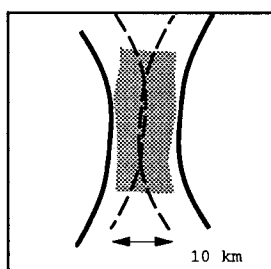
Locate box based on following rules

——▶ Extrapolation of boundaries to forecast time

——▶ Wilson-Schrieber storm locations relative to moving,
stationary and colliding boundaries (Table 1)

— — Fine tune location using winds aloft
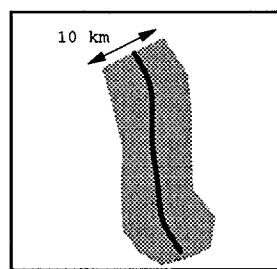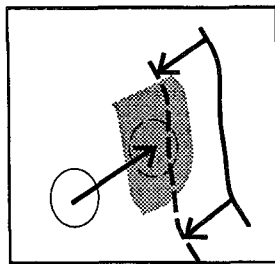
FIG. 5. Illustrations and rules for each nowcasting scenario. (a) Cell extrapolation, (b) thunderstorm initiation by boundaries, (c) cell intensification, and (d) combined thunderstorm initiation and extrapolation. Explanation of graphics are given in the legend at the top.

C) Cell Intensification by Boundaries

Issue thunderstorm forecast if;

→ Extrapolation of <30dBZ cell and boundary intersect

Locate box based on following;

→ Thunderstorm will be located with boundary

D) Combined thunderstorm initiation and extrapolation of thunderstorms already associated with boundary.
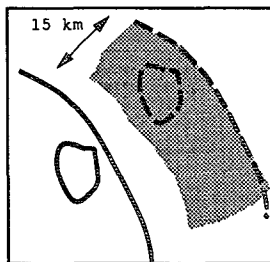
Issue forecast for thunderstorms UNLESS;

‒ ‒ Boundary is moving into stable air mass

Locate box based on following rules

→ Extrapolation of boundary and thunderstorm location to forecast time

→ Wilson-Schrieber storm locations relative to moving, stationary and colliding boundaries (Table 1)

→ If the existing cells are moving away from the boundary treat them as in A) cell extrapolation

‒ ‒ Fine tune using winds aloft

FIG. 5. (Continued)

odology was developed. The nowcasting experiments are exploratory and the nowcast methodology is evolutionary. The following nowcasting guidelines are specific to the Denver vicinity and would likely need some modification for other climatic regions. Experience by the authors in nowcasting activities in Florida and tropical northern Australia indicate many similarities. Because of more moisture in these more tropical locations, storm initiation with moving boundaries and horizontal rolls was more common.

The nowcasts in this paper are based primarily on radar data and visual cloud observations. High-resolution, quality surface measurements of temperature and moisture were not available during 1989 and 1990. The forecasters generally used mesonet and sounding data in only the more obvious situations. For instance, if the morning sounding was very dry and stable and surface moisture reports did not indicate any increase in moisture following the sounding time, the forecaster would most likely not nowcast storm initiation with boundaries. Monitoring cumulus clouds was particularly useful for assessing changing stability conditions. An increase in cumulus cloud development associated with horizontal rolls, stationary boundaries, and along moving boundaries was used as a favorable indication of storm initiation. These clouds are indirect evidence of regions of deep boundary-layer moisture which was shown by Mueller et al. (1993) to be important for storm initiation. For this monitoring activity satellite cloud imagery was often of limited usefulness since, at best, it was available half hourly and there were frequent errors with earth registration of the data.

The nowcasting guidelines are divided into four scenarios: a) thunderstorm extrapolation, b) thunder-

storm initiation by a boundary, c) intensification of a weak cell (<30 dBZ) by a boundary, and d) combined thunderstorm initiation by a boundary and extrapolation of a thunderstorm already associated with the same boundary. Illustrations and rules for each scenario are summarized in Fig. 5 and discussed here. The narrative in Fig. 5 attempts to indicate actions that are quantitative from subjective by using solid arrows and dashed lines, respectively. Before issuing a nowcast, the forecaster would decide which scenario to follow. The scenario was recorded along with the nowcast. The following subsections describe each scenario.

a. Extrapolation (A)

For this scenario the forecaster examined each cell and decided if it would remain the same (A1), dissipate (A2), or grow (A3). Typically when the forecaster decided to issue a nowcast polygon it would be larger than the expected size of the cell to allow for errors in echo movement and uncertainty in forecasting growth.

Most of the cells in the nowcast area are single- or multicellular storms that are short lived. Smaller cells tend to have shorter lifetimes than larger ones. Lacking completion of a study on cell lifetime versus cell size, quantitative rules were not established for when to dissipate a storm. In practice, cells with 30-dBZ core diameter <10 km were generally not extrapolated to the next 30-min forecast period. In addition, Doppler velocity signatures were monitored for indications of surface divergence associated with downdrafts in the cell.

The front range of the Rocky Mountains lies just west of the nowcast area (see Fig. 2). While many thunderstorms are present in these mountains they
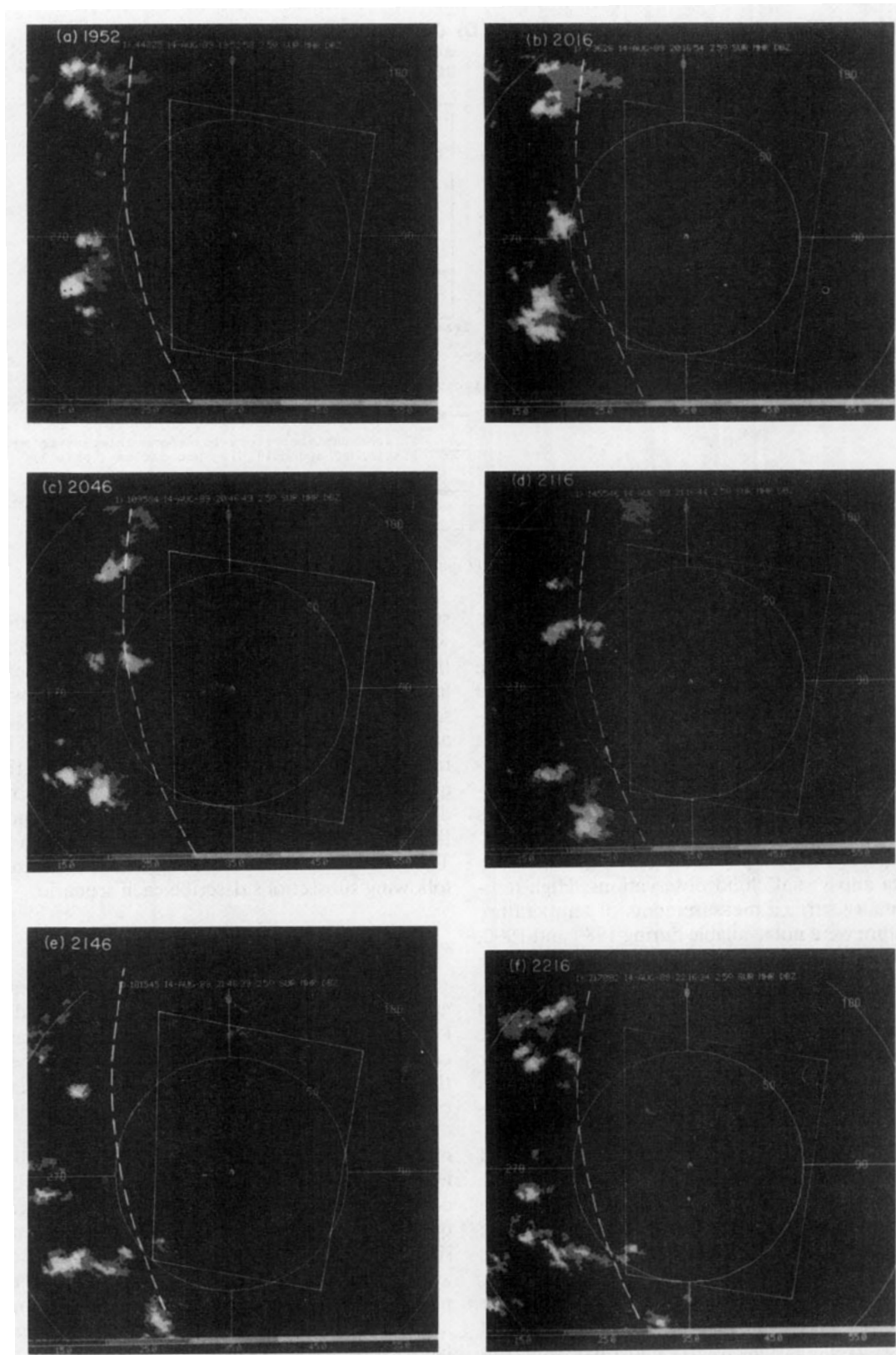
FIG. 6. Example of cells dissipating as they move eastward from the mountains to the plains. The data are for an elevation angle of 4.0° at ~30-min intervals from the MHR on 14 August 1989. The heavy-dashed white line delineates the mountains to the west from the plains. This line roughly follows the 6000-ft contour along the west side of the forecast area. The forecast area is outlined by the thin solid line. Reflectivity factor values are shown in dBZ as indicated by the scale at the bottom. (a) 1952 UTC, (b) 2016, (c) 2046, (d) 2116, (e) 2146, and (f) 2216.

usually dissipate as they move onto the plains. Figure 6 is an example of this phenomena. Although there are a number of 30+ dBZ cells over the mountains that are moving eastward, they all dissipate as they reach the forecast area. Regardless of size, cells over the mountains were nearly always nowcast to dissipate before reaching the nowcast area. The exceptional case was a cell extrapolated to move over an existing convergence line on the plains or a cell which continued to live in association with its own gust front that had moved onto the plains. Figure 7 is an example of a storm intensifying as it moves from the mountains to the plains along a convergence line. Actually there are two convergence lines, the one to the north is moving rapidly south and thus soon leaves behind the cell seen

at 2225 UTC (Fig. 7a) moving off the mountains just behind the boundary. This cell then dissipates as it moves onto the plains. The southern boundary is stationary and the cell moving off the mountains over it is able to grow and intensify.

Nowcasting storm growth was particularly difficult. Figure 8 is an example of the development of a large storm over a 1-h time period (storm northwest of radar). In this case the storm initially forms behind a boundary moving eastward and continues to grow as the storm generates an outflow on its west side and another boundary approaches from the south. In this case, strong surface convergence was evident in Doppler velocity signatures associated with each convergence line. Often storm growth nowcasts were based on
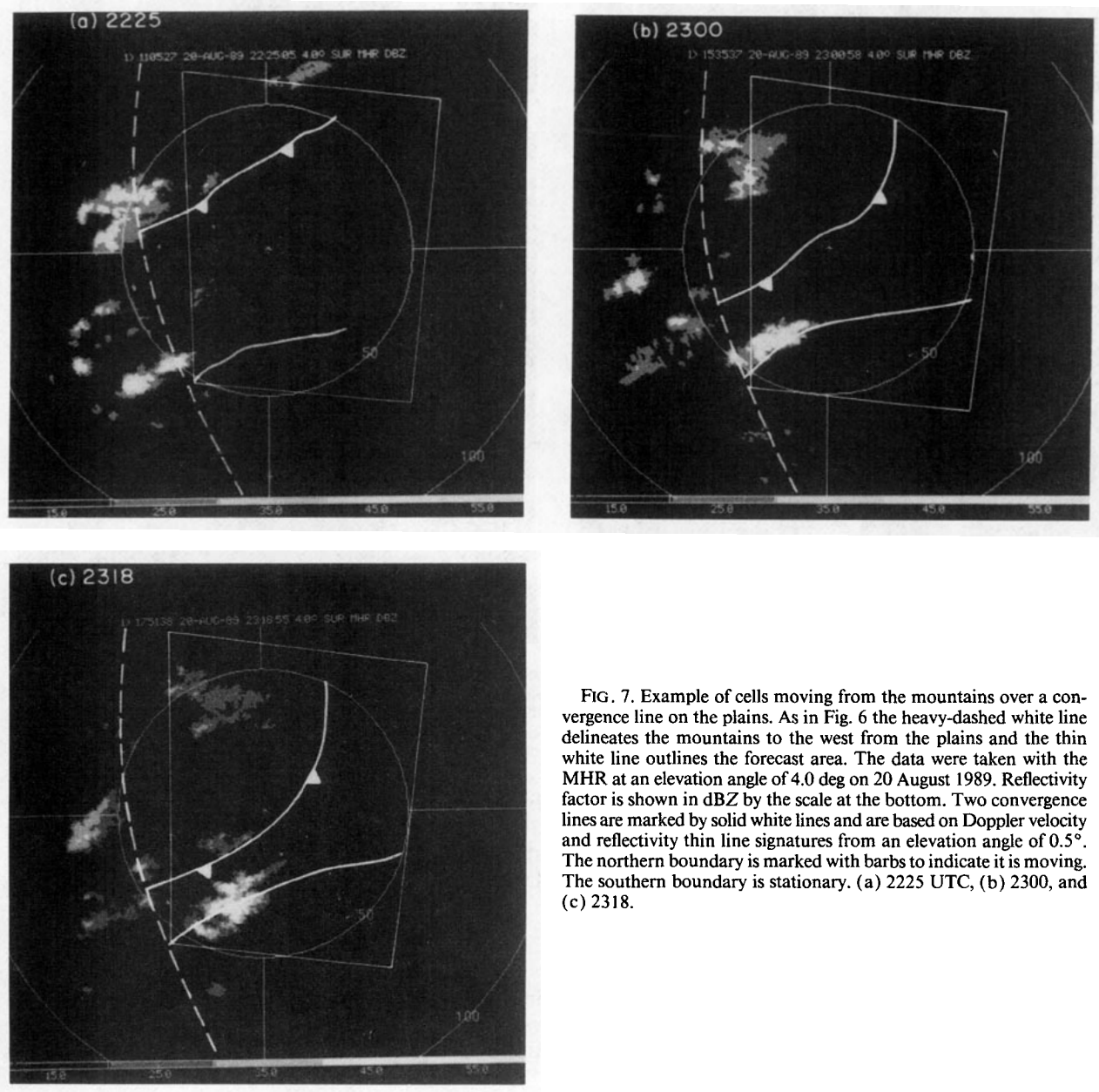
FIG. 7. Example of cells moving from the mountains over a convergence line on the plains. As in Fig. 6 the heavy-dashed white line delineates the mountains to the west from the plains and the thin white line outlines the forecast area. The data were taken with the MHR at an elevation angle of 4.0 deg on 20 August 1989. Reflectivity factor is shown in dBZ by the scale at the bottom. Two convergence lines are marked by solid white lines and are based on Doppler velocity and reflectivity thin line signatures from an elevation angle of 0.5°. The northern boundary is marked with barbs to indicate it is moving. The southern boundary is stationary. (a) 2225 UTC, (b) 2300, and (c) 2318.

FIG. 8. Example of sustained cell growth associated with strong surface convergence. Data are from the FL-2 radar on 16 July 1988 at an elevation angle of 1°. The convergence lines (white lines) were based on color Doppler velocity and radar reflectivity displays which used lower reflectivity thresholds. The boundary t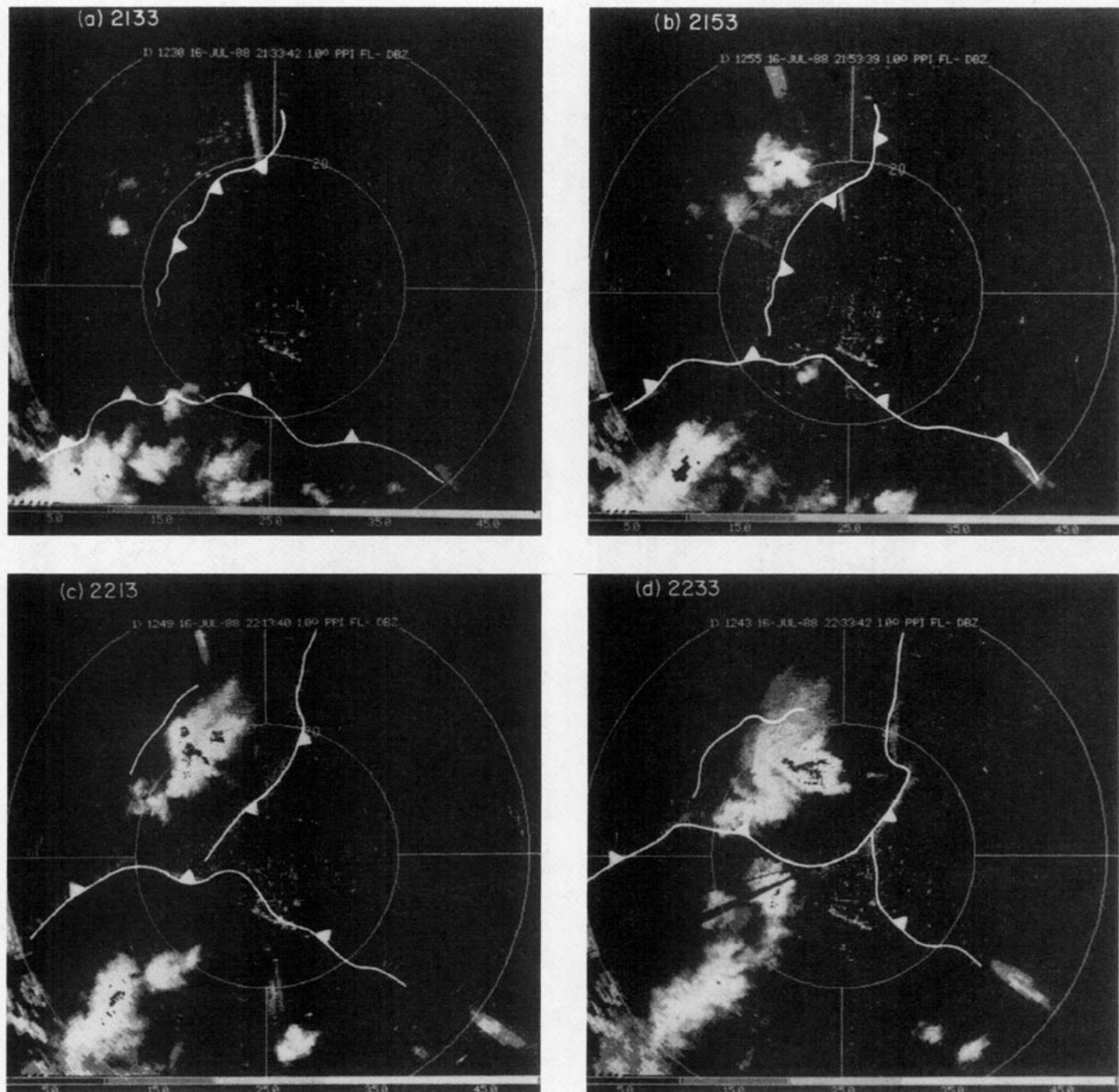o the northwest in (c) and (d) is stationary the other boundaries are moving as indicated. (a) 2133 UTC, (b) 2153, (c) 2213, and (d) 2233.

Doppler velocity signatures suggestive of strong (quantitative rule not available) surface convergence.

Another situation where growth was nowcast was when two or more cells appeared to be merging (Wescott 1984). The guidelines for extrapolation nowcasts are given in Fig. 5A.

b. Initiation by boundaries (B)

A summary of the temporal and spatial relationship of thunderstorm initiation associated with boundaries from Wilson and Schreiber (1986) is given in Table 1. The guidelines (summarized in Fig. 5b) for nowcasting storm initiation in this section are largely based on this table.

1). STATIONARY BOUNDARIES (B1)

For the category "stationary boundaries," Table 1 indicates that when storms form they are typically within 10 km of the boundary. The challenge with stationary boundaries was to properly anticipate when

TABLE 1. Summary of Wilson and Schreiber (1986) results as applied to thunderstorm nowcasting. Boundaries which meet with intersection angles < 30° are defined as collisions; otherwise as intersections.

	Boundary categories			
	Stationary	Moving	Colliding	Intersecting
Percent initiate storms (number of boundaries)	60 (42)	65 (124)	63 (19)	54 (22)
Location of storms relative to boundary (km)	0–10	0–15 behind	0–5	0–5
When storms form relative to boundary	n/a	10–40 min after passage	15–30 min after collision	15–30 min after intersection

storm initiation would begin. A stationary boundary may exist for hours before producing storms, if at all. An example and detailed study of storm initiation with a stationary boundary is given by Wilson et al. (1992). In this case it is shown that a stable environment not favorable to storm initiation is modified locally along the boundary to produce an environment favorable for storm initiation. The best way to anticipate storm development was to monitor cloud development visually or with satellite imagery and/or monitor upper-radar elevation angles for the first appearance of precipitation echo. When placing the forecast polygon the environmental steering winds were considered to anticipate the direction in which the storms would move.

2). MOVING BOUNDARY (B2)

For the category "moving boundaries," Table 1 indicates that storms typically form 0–15 km behind the boundary or 10–40 min after boundary passage. Figure 9 is an example of thunderstorm initiation behind an advancing convergence line that closely fits these guidelines. The time for cell initiation is shown in parentheses to the right of each new cell number. The time for cell initiation is defined as the time after boundary passage for the cell to reach 30 dBZ. In Fig. 9, the time to storm initiation varied from 2 to 35 min. Note in Fig. 9 the initiation of storms is sporadic both in time and space as the boundary advances. From Mueller et al. (1993), it is believed that this variability results from boundary-layer moisture and temperature variations on a horizontal scale of a few kilometers as would be associated with boundary-layer convective rolls and on scales of tens of kilometers associated with mesoscale features. Storm initiation in regions of negative static stability appeared to be very sensitive to the depth of the boundary-layer moisture. As discussed earlier, visual observations were used to assess thunderstorm potential. If the boundary were moving into a region of towering cumulus it was highly likely storms would develop. At close range (within ~50 km) the radar can often detect cumulus congestus clouds. Figure 10 is an example of the rapid development of two storms as a gust front moves into a field of cumulus clouds. The cumulus clouds are apparent in Fig. 10a

as small echoes of 0–15 dBZ at an elevation angle of about 3°. The gust front was drawn on this ~3° elevation scan based on its thin-line location at lower elevation angles. The echoes reached 30 dBZ within only 5–10 min after boundary passage, presumably because the clouds were already in an advanced stage of development.

Kessinger and Mueller (1991) have reported on the initiation of storms when a moving boundary intersects horizontal rolls. These collisions often produce storms in humid, unstable conditions; however, these conditions usually do not occur in Colorado. When lines of cumulus clouds are associated with horizontal rolls this is identical to the example given in Fig. 10. Figure 11 is an example from Colorado where a moving boundary is intersecting horizontal rolls oriented normal to the boundary. Satellite imagery in this case showed north–south lines of cumulus clouds in advance of the moving boundary. Figure 11d shows three north–south lines of storms that formed along the original position of the convergent region between rolls. The westernmost line seen at 2343 UTC in Fig. 11d did not show an obvious prior roll in Fig. 11a although the 1.2° elevation angle which was used in Fig. 4 does show this roll. The forecasters issued nowcast polygons in these situations only when they had evidence that there were cumulus clouds along the rolls and/or the horizontal roll was relatively intense as indicated by radar reflectivity factor and/or Doppler velocity.

3). COLLIDING BOUNDARIES (B3)

Table 1 shows that storms initiated by colliding boundaries tend to form within 5 km of the boundary and 15–30 min after collision. This was one of the easier forecast situations since timing and location ambiguities are decreased. All collisions do not initiate storms; Table 1 shows 63% for Colorado during the summer of 1985. This percentage obviously depends on the average climatic stability conditions; however, because collisions can generate very strong updrafts (Mahoney 1988) storms can be initiated in relatively stable conditions where they otherwise would not form. Some of the more intense storms tend to form with colliding boundaries. If storms or even cumulus humilis
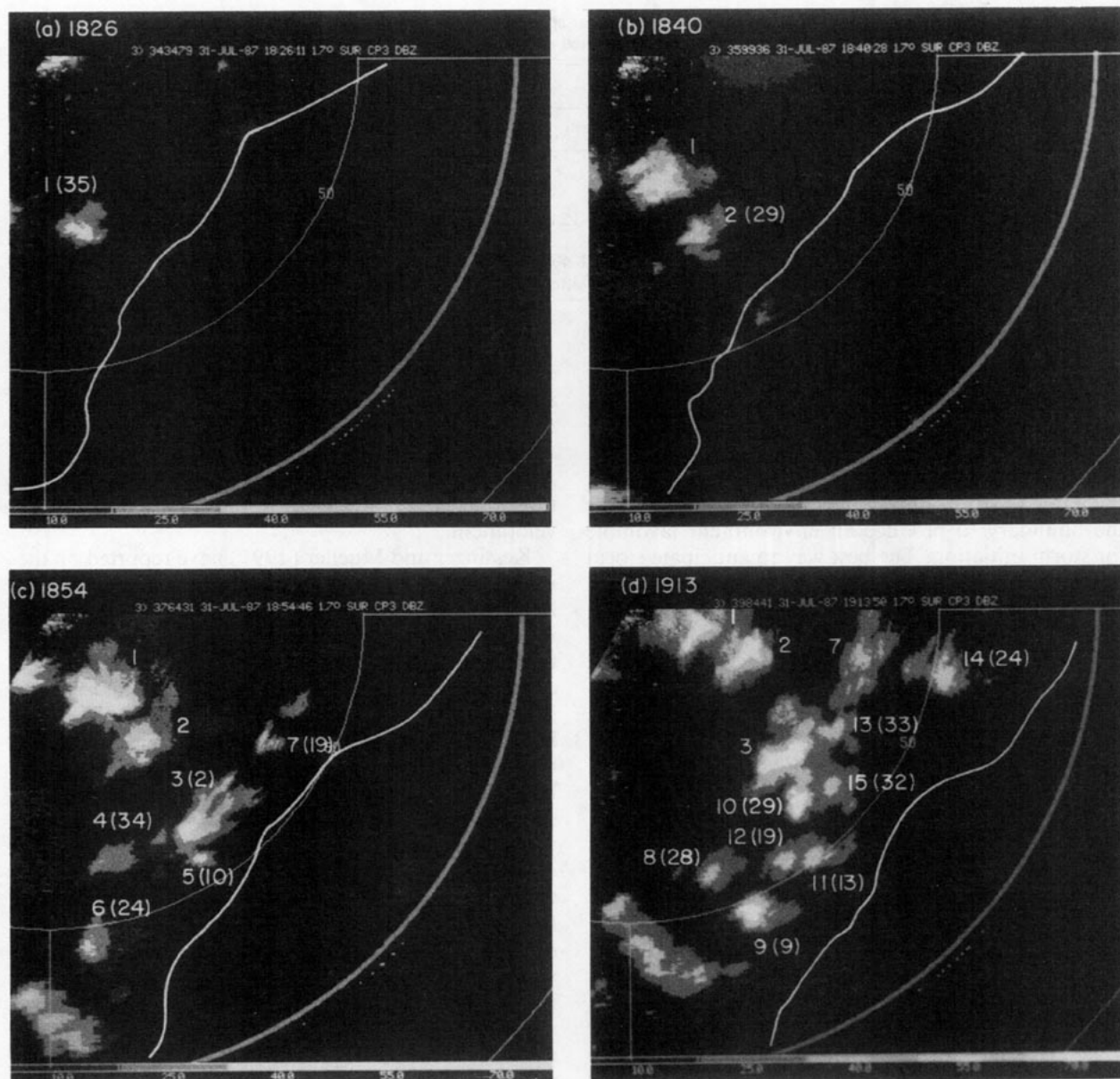
FIG. 9. Example of a moving boundary initiating storms. Data are from the CP-3 Doppler radar on 31 July 1987 at an antenna elevation angle of 1.7°. For convenience storms are numbered. Numbers in parentheses to the right of new cell numbers are the elapsed time (min) for the cell to reach 30 dBZ after the boundary passed that location. The moving boundary is based on a reflectivity thin line and Doppler velocity convergence signature at 0.9° from color displays with a lower reflectivity threshold. Radar reflectivity factors are given by the gray scale at the bottom. The first range ring is at 50 km. (a) 1826 MDT (0026 UTC), (b) 1840, (c) 1854, (d) 1913.

clouds were present in the anticipated collision area or if either were associated with at least one of the boundaries, storms were forecast following the collision. In fact, if towering cumulus are present in the collision area, the time to first storm will often be less than 15 min and may actually occur before the collision. Conversely, if the collision occurred under a deck of middle to high clouds and cumulus clouds were not present, storms were not forecast. Guidelines for forecasting

storm initiation with convergence lines are summarized in Fig. 5b.

c. Cell intensification by boundaries

Weak cells (less than 30 dBZ) extrapolated to move over a convergence line were forecast to increase in intensity > 30 dBZ. The nowcast typically required monitoring upper-elevation angles for weak echo. In
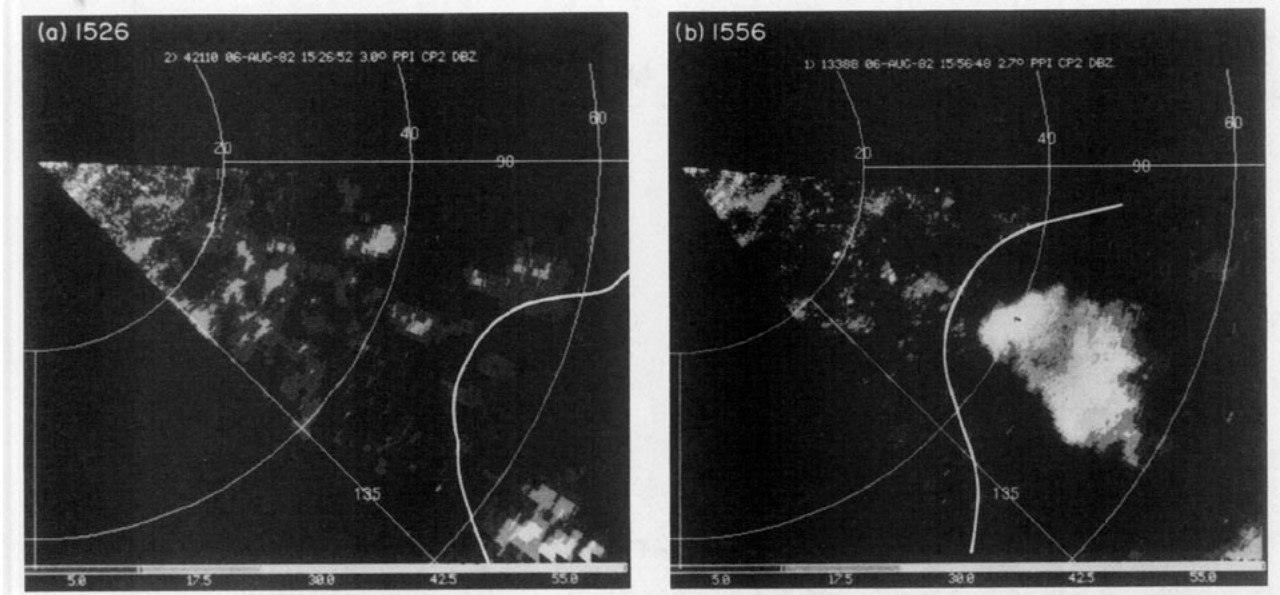
FIG. 10. Example of a gust front initiating storms as it moves through a field of cumulus clouds. Data are from the CP2 radar on 6 August 1982. (a) 1526 MDT (2126 UTC); the data are at an elevation angle of 3.0°. The solid white line indicates the location of the gust front moving westward. Its location is based on a reflectivity thin line at an elevation angle of 0.5°. The cumulus clouds are evident as echo of ~0 to 15 dBZ. (b) same as (a) except at 1556 MDT.

this situation it was assumed that storm initiation (intensification) was due to the convergence line reinforcing updrafts into the weak echoes. Anvil echo less than 30 dBZ moving over a convergence line was not forecast to intensify. The guidelines for nowcasting cell intensification by a boundary are shown in Fig. 5c.

d. Extrapolation and initiation

In this scenario storms are already being initiated by a boundary. The forecaster continued to nowcast storm initiation using the guidelines in Table 1. The only exception was if the forecaster had evidence that the boundary was moving into a stable air mass. The primary decision was how to handle the existing cells. In the case where the steering level winds are advecting the cells in the general direction of the boundary motion, the storms tended to be long lived and remained 0–15 km behind the boundary. In the case of colliding boundaries or stationary boundaries the new cells tended to move away from the boundary, but generally at a speed less than the steering-level winds. Occasionally, a moving boundary moved in a direction considerably different than the storm steering-level winds. This was the situation in Fig. 9 where the boundary was moving from the northwest and the cells were moving from the south. Cells 1, 2, and 3 in Fig. 9 had lifetimes of about 1 h, where the others were typically less than 30 min. The general rule for nowcasting the lifetime and location of cells moving away from the boundary was the same as given in section 4a for extrapolations. New storms continued to be nowcast us-

ing the rules for moving boundaries. The guidelines for nowcasting thunderstorms for combined thunderstorm initiation and extrapolation are summarized in Fig. 5d.

5. Nowcasts

a. Procedures

During the summers of 1989 and 1990 the forecasters issued polygons where thunderstorms were nowcast to be in 30 min. Actually the nowcasts were for radar reflectivity factors > 30 dBZ in 1989 and >40 dBZ in 1990. The change from 30 to 40 dBZ was for operational reasons. The aircraft controllers felt 40 dBZ was more closely matched to aviation hazards than 30 dBZ. The nowcast region as shown in Fig. 2 occupied about 8000 km^2 around Stapleton Airport. Figure 12a is a black and white example of the display that was sent to the FAA controllers. The 30-min nowcasts were issued at 20-min intervals in 1989 and 30-min intervals in 1990. The polygons were drawn using the guidelines in Fig. 5. Nowcasts and verification were for a radar elevation angle of 4° because of an operational decision to provide the aircraft controllers with reflectivity data for this angle. This presented some forecast problems in stratiform regions trailing convective systems since brightband echoes would often exceed 30 dBZ. Forecasts were made daily from 1300 to 1900 MDT from 14 August through 7 September 1989 and 19 June through 27 July 1990. Extensions to 2100 MDT often occurred if storms were still active at 1900.
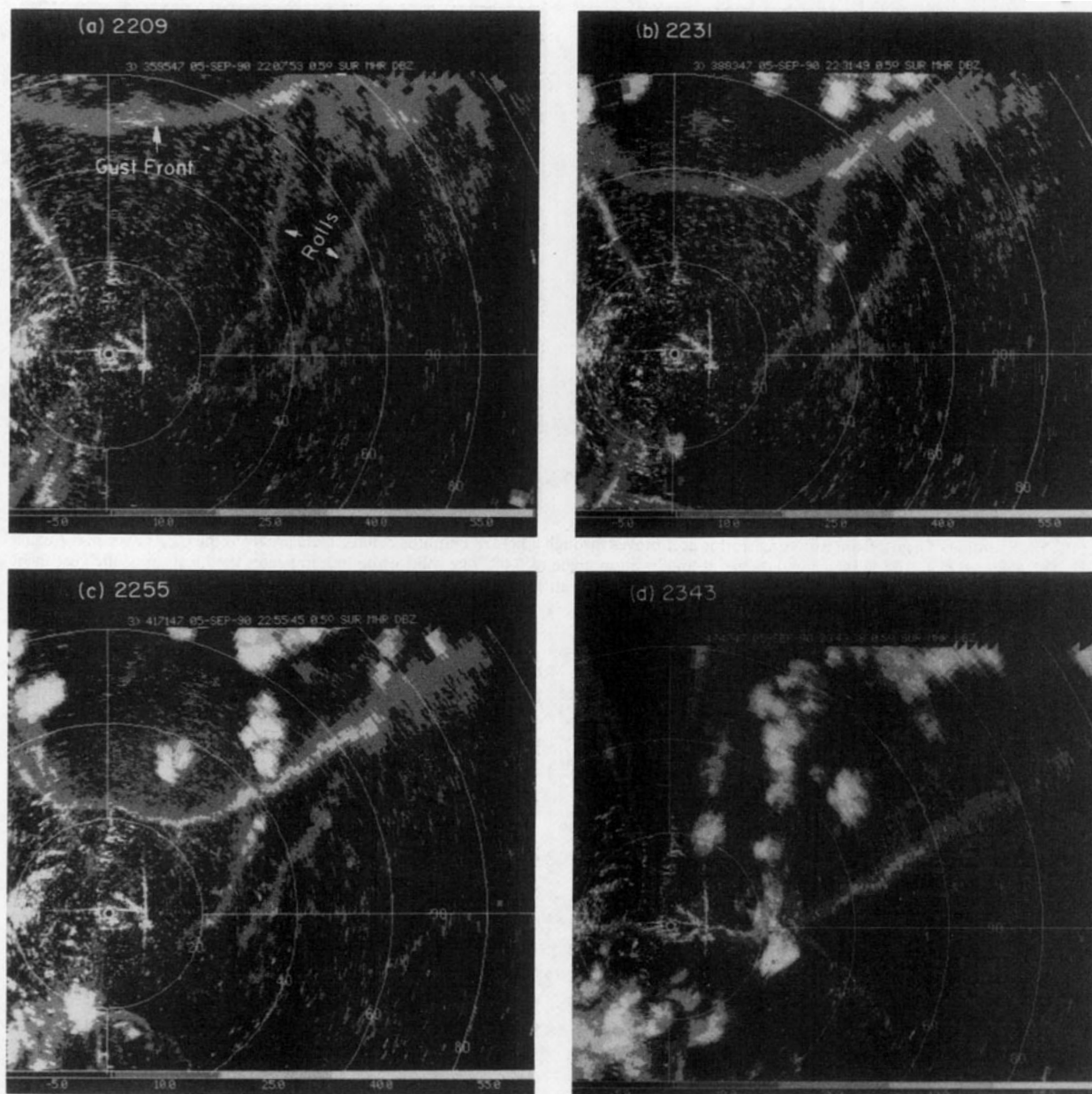
FIG. 11. Example of storm initiation by a moving boundary (gust front) intersecting lines of cumulus clouds associated with horizontal convective rolls. The data are from the MHR on 5 September 1990 at an elevation angle of 0.5°. (a) 2209 UTC, (b) 2231, (c) 2255, and (d) 2343.

During 1989, NWS and AWS personnel participated in the exercise. A total of six people were lead forecasters during the two summers. At least one of the authors was present on all forecast days and provided cohesion and training. The statistics presented here are meant to give a feel for how the forecaster, using techniques previously described, compared with persistence and extrapolation forecast methods, and to discern areas where improvements need to be made. The statistics are not necessarily reproducible measures of

nowcasting ability (i.e., another group of forecasters after training may or may not have the same ability).

To compare the human nowcasts with those of persistence and extrapolation, the nowcast region was overlaid with a 5 × 5-km grid of squares. If >1 km² of a 5 × 5-km square contained >30*[4] dBZ the 5 × 5-km square was declared to contain a thunderstorm.

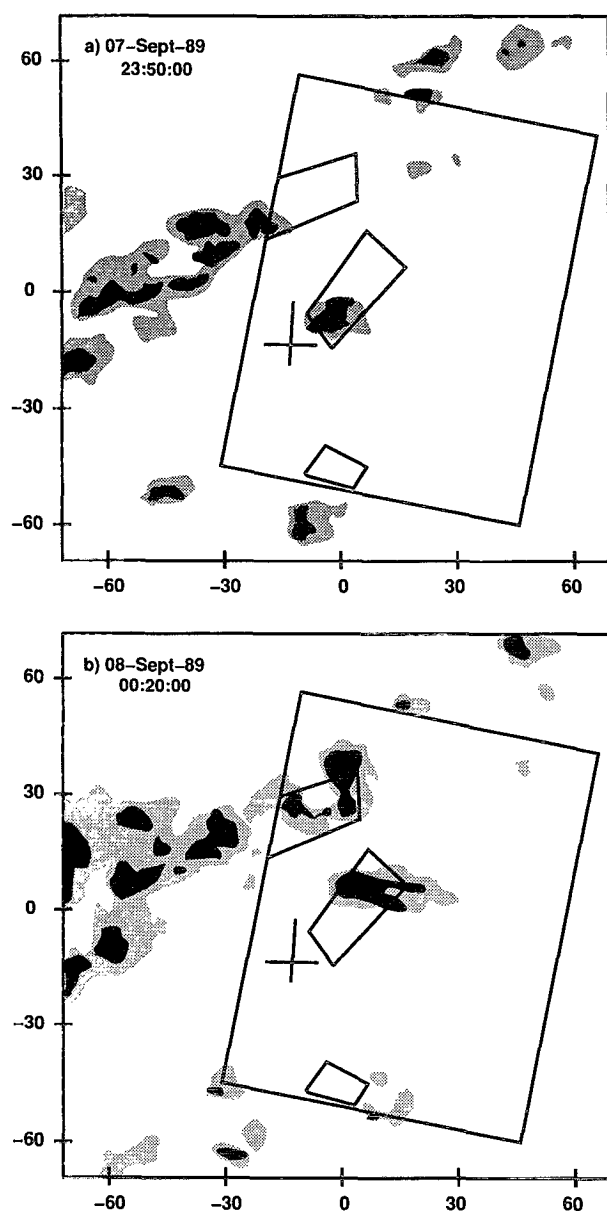[4] 30* refers to 30 dBZ in 1989 and 40 dBZ in 1990.

FIG. 12. Display showing precipitation and nowcast polygons for nowcast and valid times. Precipitation shadings are for >18 and >30 dBZ. The large rectangle is the nowcast domain. The grid marks around the figure boundary are in kilometers. The two intersecting lines represent the north–south and east–west runways at Stapleton airport. (a) Precipitation display at 2350 UTC. The polygons are 30-min nowcasts valid at 0020 UTC. This display in color is similar to that sent the FAA controllers. (b) Precipitation validation at 0020 UTC of the nowcasts in (a).

The same procedure was used for the nowcast polygons. Persistence forecasts simply compared the 5-km gridded precipitation map at nowcast time with that 30 min later at verification time. The extrapolation forecasts were based on movement vectors computed in

real time (Garant and Chornoby 1990). The vectors were based on cross-correlating radar scans separated by 6 min. A vector was determined for each 28 × 28-km^2 area of a radar scan after converting 1-km gridded reflectivity-field data to a binary echo/no-echo field. An echo was defined as a reflectivity greater than 30 dBZ. After smoothing the vector field, 30-min linear extrapolation forecasts were made. Ideally the extrapolation forecasts should be based on 30-min rather than 6-min movement vectors (Wilson 1966); however, some of the highly perishable small-scale features are smoothed by reducing the data to echo or no-echo before computing correlations. Extrapolation vectors were available only for 1990.

b. Results

A total of 315 nowcast "polygons" were issued during the two years. Table 2 shows the median size, percent that verified correctly, and for those that verified correctly the average percent of the polygon covered by thunderstorm echo. Here, 61% and 50% of the polygons were correct nowcasts in 1989 and 1990, respectively; however, much of the polygon did not contain thunderstorms (average coverage 29% and 15%).

There were 98 regions in 1989 and 112 regions in 1990 where a thunderstorm occurred but was not nowcast. A "region" refers to an individual thunderstorm or cluster of thunderstorms. Importantly, 60% of these regions immediately adjoined a nowcast polygon. Figure 12b is an example of this common phenomena. There are a variety of reasons for these "close misses" which will be discussed later in this section. Two missed nowcast regions are visible in Fig. 12b. The first is the >30 dBZ echo extending northward out of the northern nowcast polygon and the second is echo extending east and west outside of the central nowcast polygon.

The forecasters noted the reason or scenario (Fig. 5) for each polygon issued. Table 3 shows the number of nowcasts issued for each scenario and the percent that verified correctly. Extrapolation of existing cells was part of the nowcast reasoning in 82% of the cases and boundary initiation of cells in 39% of the cases. Both scenario types were occasionally used to make nowcasts, accounting for the total to exceed 100%.

TABLE 2. 1989 and 1990 forecast results. "Correct" refers to the percent of polygons that were observed to contain at least 1 km^2 of thunderstorm echo. "Average coverage" refers to the average amount of thunderstorm echo within the polygon.

	1989	1990
Number of boxes	155	160
Median box size (km^2)	209	190
Correct (%)	61	50
Avg. coverage (%)	29	15

TABLE 3. Statistics on verification of nowcast polygons for each of the forecast scenarios (described in the text and Fig. 5). The "% verify" indicates the percent of polygons that correctly forecast thunderstorm echo.

Forecast scenario	1989		1990	
	# cases	% verify	# cases	% verify
A2. Thunderstorm extrapolation	72	68	63	51
A3. Thunderstorm extrapolation with echo growth	26	60	31	55
B. Thunderstorm initiation by boundary	26	50	30	27
C. Less than 30*-dBZ cell intensifies to thunderstorm as it moves over boundary	12	25	4	25
D. Combined thunderstorm initiation and extrapolation of thunderstorms already associated with boundary	21	81	31	71

Those nowcasts that included both extrapolation and boundary initiation of storms were the most likely to be correct. While not involving many cases, scenario C (intensification of weak cells by boundaries) only verified correctly 25% of the time. All others with the exception of nowcasting initiation of 40-dBZ cells in 1990 by a boundary were correct at least 50% of the time.

Typically the nowcast logic was correct; however, errors often occurred in the placement of the polygon, similar to what was previously discussed for the northern two polygons in Fig. 12b. This was the case for both thunderstorm initiation nowcasts and thunderstorm extrapolation nowcasts.

The procedures for manually identifying these features and obtaining extrapolations was rather crude and prone to human errors. The forecasters felt that greater automation of this activity and research on the best way to extrapolate features for 30 min would significantly improve extrapolations and help reduce the number of close misses.

Table 4 compares the human nowcasts with persistence and extrapolation techniques for 1989 and·1990. This table contains contingency tables and statistical parameters, as defined by Donaldson et al. (1975), for probability of detection (POD), false-alarm ratio (FAR), and critical success index (CSI). The numbers in the contingency tables refer to the number of 5 × 5-km squares. For example, in Table 4 there were 1226 5 × 5-km squares where >30 dBZ (thunderstorm) was nowcast to occur and it was observed to occur. Note the very high number of nowcasts for "no thunderstorm" and "none" that were observed. It could be argued that other statistical techniques better represent the "true" nowcast skill. For example, the CSI index does not take into account correct nowcasts of "no thunderstorms." Also, no credit is received if the nowcasts are slightly off in their timing and/or placement. New techniques that will factor time and space errors into the evaluation procedure are being tested. The intent in this paper is to use a standard evaluation score to compare different forecast techniques.

The human CSI score was better than persistence or extrapolation forecasts primarily due to a higher POD score. Because both persistence and extrapolation forecasts are based on existing thunderstorms, the human forecaster demonstrated skill in nowcasting initiation of thunderstorms. The nowcasts in 1989 were considerably better than those in 1990 as determined by the lower FAR and slightly higher POD. The lower-skill scores in 1990 are probably due to changing the definition of a thunderstorm from 30 to 40 dBZ. Table 2 shows that the average size of the nowcast polygon decreased only 9% from 1989 to 1990 while the average coverage of correctly verifying reflectivity dropped from 29% to 15%. Because of the smaller scales of 40-dBZ

TABLE 4. Contingency tables for the human, persistence, and extrapolation nowcasts for 1989 and 1990. Here y and n refer to yes and no, respectively, that 30-dbZ echo was nowcast or observed (40 dBZ for 1990). Probability of detection (POD), false-alarm ratio (FAR), and critical success index (CSI) are included.

nowcast	Human observed		Persistence observed		Extrapolation observed	
	y	n	y	n	y	n
			1989			
y	1 226	2 591	516	866		
n	757	57 501	1 401	52 110		
	POD = .62		POD = .27			
	FAR = .68		FAR = .63			
	CSI = .27		CSI = .19			
			1990			
y	550	3 003	113	579	150	450
n	451	64 737	883	67 733	830	70 760
	POD = .55		POD = .11		POD = .15	
	FAR = .85		FAR = .84		FAR = .75	
	CSI = .14		CSI = .07		CSI = .10	

echo compared to 30-dBZ echo, their occurrence and lifetime is inherently less and more difficult to nowcast.

The forecasters felt that except for long-lived large cells they had little ability to nowcast cell intensity. Research and analysis tools are needed to help determine which regions of existing cells will undergo growth and which will undergo dissipation. The relationship of cells to surface convergence features is important. Improved conceptual models of cell motion and growth are needed.

The three most interesting findings are that 1) human forecasters performed better than both persistence and extrapolation forecasts, 2) 60% of the missed forecast regions immediately adjoin a nowcast polygon, and 3) the forecasts for thunderstorms of 40 dBZ or more were significantly less accurate than those for 30 dBZ.

6. Discussion and future plans

The reader is reminded that the purpose of this paper is to examine the ability to make 30-min space-specific nowcasts of thunderstorms. The results are primarily applicable to weakly forced synoptic situations where storms are typically small and short lived as are very common in the southeastern United States during the summer and in semitropical and tropical regions of the world. It has been shown that monitoring the location of boundary-layer convergence lines with sensitive Doppler radars (similar to the WSR-88D), together with monitoring cloud development in the vicinity of these boundaries provides the capability to make spatially detailed nowcasts of thunderstorm initiation. There is much room for improvement, however. Forecasters often had difficulty in precisely timing and placing the location of storm initiation. They had even more difficulty in nowcasting the evolution of existing storms. Three reasons for these difficulties are: 1) there is a basic deficiency in our knowledge of the details of storm initiation and evolution, 2) there is a need for detailed observations of boundary-layer thermodynamics and more detailed observations of cumulus cloud location and growth, and 3) many of the forecaster activities were manually intensive and prone to error.

With regard to item 1, storm initiation can be very sporadic in time and space. Small-scale variations in boundary-layer thermodynamics may be responsible for this, however, the forecasters often felt other unknown forces were acting. Research in this area will combine numerical modeling and observational studies. Data from the Convection and Precipitation/electrification Experiment (CaPE) which took place in Florida during 1991 may provide some answers. One of the primary goals of CaPE was to study storm initiation utilizing a wide variety of measurement systems. Nowcasting details of storm movement and intensity

changes are also not well understood. Statistical research is presently in progress to determine cell lifetime as a function of cell size and intensity. In addition, using the cell identification and quantification program described by Dixon and Wiener (1992), cell parameters such as height of the mass-weighted reflectivity core, echo-top trend, echo-intensity trend, surface divergence, and storm rotation will be examined for prediction value.

A nonhydrostatic 2D and 3D numerical model capable of being run in near-real time is being implemented by Crook (1991). This model is a version of one developed by Clark and collaborators (Clark 1977; Clark and Farley 1984). Tests will be made to initialize the model with winds from the Mile High Doppler radar. The wind field will be derived from the single Doppler technique called TREC (tracking radar echoes by correlation) which is described by Rinehart and Garvey (1978) and Tuttle and Foote (1990). Winds are obtained by tracking very small-scale features in the clear air. The track or wind vector is determined by cross-correlating patterns separated in time by a few minutes.

With regard to item 2 (improved observations), Mueller et al. (1993) addresses the issue of boundary-layer thermodynamic measurements and conclude that three-dimensional detailed (1-3 km) measurements of boundary-layer moisture are desirable for forecasting storm initiation; currently measurements on this scale are not possible. Without detailed observations of boundary-layer moisture, temperature, and winds, monitoring cloud development in the vicinity of convergence lines is the best method for anticipating specific storm development locations along boundaries. During the nowcast experiments, cumulus cloud monitoring was primarily accomplished visually by the forecaster. This procedure would not be universally practical because of visibility restrictions in many places. Satellite imagery provides only limited utility. Images are typically only every 30 min, cloud–earth registration is often in error and cirrus clouds often obscur the lower cumulus clouds. An increased effort is planned to utilize 10-cm-wavelength Doppler radar to map the location of cumulus clouds prior to precipitation production. Field experiments in North Dakota, Hawaii, and Florida described by Knight and Miller (1992) showed that cumulus clouds when first visible to the eye were detectable at close range by sensitive Doppler radars. For S-band radars, the radar reflectivity factor of these first visible clouds was -10 to -20 dBZ. The MHR (similar to the WSR-88D) which was used in the forecasting experiments discussed here has the ability to detect a -20-dBZ signal at a range of 25 km (-13 dBZ at 60 km). Thus, by increasing the sensitivity 7 dB, it should be possible to observe the initial cumulus clouds with the radar over the entire nowcast area (range 60 km). This will allow for the almost contin-

uous and precise monitoring of all the cumulus clouds in the nowcast area. Efforts will continue to increase radar sensitivity and determine the radar's ability to detect cumulus clouds in various stages of development.

The third area planned for improvement is automation nowcaster activities that are routine and/or prone to human error. This will allow the forecaster more time to use his/her physical reasoning and pattern recognition capabilities to assess data quality, evaluate automated forecast material, and apply broad-based meteorological reasoning to the forecasts (Wilson and Carbone 1984). Beginning in 1992, the forecasters will have available automated cell (Dixon and Wiener 1992) and boundary detection (Rogers et al. 1991) algorithms. These features will be automatically extrapolated to the forecast time based on past motion. Collisions or interactions of features during the forecast period will be noted by the computer. The guidelines in Table 1 regarding the placement and timing of storm initiation will be automatically applied and storm initiation areas bounded. During this process the forecaster would have the ability to reject and/or modify automated cell detections, boundary detections, extrapolations, and storm initiation polygons.

We envision a continually evolving human/computer nowcast system where activities that become routine will be automated and the nowcaster will have more and more time to apply his/her deductive reasoning abilities to the nowcast.

REFERENCES

Achtemeier, G. L., 1991: The use of insects as tracers for "clear-air" boundary-layer studies by Doppler radar. *J. Atmos. Ocean. Technol.,* **8,** 746–765.

Alberty, R., T. Crum, F. Toepfer, 1991: The NEXRAD program past, present and future: A 1991 perspective. Preprints, *25th International Radar Meteorology Conf.,* Paris, Amer. Meteor. Soc., 1–8.

Austin, G. L., 1985: Application of pattern recognition and extrapolation techniques to forecasting. *ESA J.,* **9,** 147–156.

Barron, R., G. Gray, and J. Lutz, 1986: New Features for NCAR radars. Preprints, *23d Conf. on Radar Meteorology,* Snowmass, Amer. Meteor. Soc., JP346–JP347.

Battan, L. J., 1973: *Radar Observations of the Atmosphere.* University of Chicago Press, 324 pp.

Browning, K. A., and C. G. Collier, 1982: An integrated radar-satellite nowcasting system in the UK. *Nowcasting,* K. Browning, Ed., Academic Press, 47–61.

Carbone, R. G., J. W. Conway, N. A. Crook, and M. W. Moncrief, 1990: The generation and propagation of a nocturnal squall line. Part I: Observations and implications for mesoscale predictability. *Mon. Wea. Rev.,* **118,** 26–49.

Christian, T. W., and R. M. Wakimoto, 1989: The relationship between radar reflectivities and clouds associated with horizontal roll convection on 8 August 1982. *Mon. Wea. Rev.,* **117,** 1530–1544.

Clark, T. L., 1977: A small scale numerical model using terrain following coordinate transformation. *J. Comput. Phys.,* **24,** 186–215.

——, and R. D. Farley, 1984: Severe downslope windstorm calculations in two and three spatial dimensions using anelastic interactive grid nesting: A possible mechanism for gustiness. *J. Atmos. Sci.,* **41,** 329–350.

Crook, D. A., 1991: Small-scale moisture variability in the convective boundary layer and its implications for nowcasting. Preprints, *25th Conf. on Radar Meteorology,* Paris, Amer. Meteor. Soc., 67–70.

Dixon, M., and G. Wiener, 1993: TITAN: Thunderstorm identification, tracking, analysis, and nowcasting—A radar-based methodology. *J. Atmos. Oceanic Tech.,* submitted.

Donaldson, R. J., R. M. Dyer, and M. J. Kraus, 1975: An objective evaluation of techniques for predicting severe weather events. Preprints, *Ninth Conf. on Severe Local Storms,* Norman, Amer. Meteor. Soc., 321–326.

Doswell, G. A., 1986: Short-range forecasting. *Mesoscale Meteorology and Forecasting,* P. Ray, Ed., Amer. Meteor. Soc., 793 pp.

Doviak, R. J., and D. S. Zrnic, 1984: *Doppler Radar and Weather Observations.* Academic Press, 458 pp.

Dunn, L. B., 1990: Two examples of operational tornado warnings using Doppler radar data. *Bull. Amer. Meteor. Soc.,* **71,** 145–153.

Entrekin, H. D., J. W. Wilson, and K. D. Hage, 1969: Evaluation of the Atlantic City mesonet for short range prediction of aviation terminal weather. *J. Appl. Meteor.,* **8,** 473–483.

Evans, J. E., and D. H. Turnbull, 1985: The FAA/MIT Lincoln Laboratory Doppler weather radar program. Preprints, *Second International Conf. of the International Weather System,* Montreal, Amer. Meteor. Soc., 73–76.

Garant and Chornoby, 1990: The Lincoln Laboratory TDWR storm movement prediction algorithm: Top level description. MIT Lincoln Lab. Memo, No. 43PM-wx-0028, 52 pp. [Available from Lincoln Lab. Program Mgr., Lexington, Ma.]

Hardy, K. R., D. Atlas, and K. M. Glover, 1966: Multi-wavelength backscatter from the clear atmosphere. *J. Atmos. Sci.,* **36,** 1077–1091.

Harvey, L. O., Jr., K. R. Hammond, C. M. Lusk, E. F. Gross, 1992: The Application of Signal Detection Theory to Weather Forecasting Behavior. *Mon. Wea. Rev.,* **120,** 863–883.

Keeler, R. J., B. W. Lewis, and G. R. Gray, 1989: Description of NCAR/FOF Cp-2 meteorological Doppler radar. Preprints, *24th Conf. on Radar Meteorology,* Tallahassee, Amer. Meteor. Soc., 589–592.

——, ——, R. K. Bowie, and J. R. Vinson, 1991: NCAR's c-band Doppler radars. Preprints, *25th Conf. on Radar Meteorology,* Paris, Amer. Meteor. Soc., 859–862.

Keenan, T., R. J. Potts, and J. Wilson, 1991: The Darwin area forecast experiment: Description and preliminary results. *Aust. Meteor. Mag.*, **39**, 211–222.

——, ——, and T. Stevenson, 1992: An evaluation of the Darwin area forecast experiment storm occurrence forecasts. *Wea. Forecasting*, **7**, 515–523.

Kessinger, C. J., C. K. Mueller, 1991: Background studies and nowcasting Florida thunderstorm activity in preparation for the CaPOW forecast experiment. Preprints, *25th Conf. on Radar Meteorology*, Paris, Amer. Meteor. Soc., 416–419.

Knight, C. A., and L. J. Miller, 1993: First radar echoes from cumulus clouds. *Bull. Amer. Meteor. Soc.*, submitted.

Lauritsen, P., Z. Mulekmadanic, C. Movel, and R. McBeth, 1987: The cross-chain LORAN atmospheric sounding system (CLASS). Preprints, *Sixth Symposium on Meteorological Observations and Instrumentation*, New Orleans, Amer. Meteor. Soc., 340–343.

Lutz, J. S., S. E. Yuter, and J. W. Wilson, 1989: The nowcaster workstation for analyzing four-dimensional radar data. Preprints, *24th Conf. on Radar Meteorology*, Tallahassee, Amer. Meteor. Soc., 216–219.

Mahoney, W. P., III, 1988: Gust front characteristics and the kinematics associated with interacting thunderstorm outflows. *Mon. Wea. Rev.*, **116**, 1474–1491.

Mueller, C. K., and R. E. Carbone, 1987: Dynamics of a thunderstorm outflow. *J. Atmos. Sci.*, **44**, 1879–1898.

——, and J. W. Wilson, 1989: Evaluation of the TDWR nowcasting experiment. Preprints, *24th Conf. on Radar Meteorology*, Tallahassee, Amer. Meteor. Soc., 224–227.

——, ——, and N. A. Crook, 1993: Utility of soundings and mesonets to forecast thunderstorm initiation. *Wea. Forecasting*, **8**.

Mueller, E. A., and R. P. Larkin, 1985: Insects observed using dual-polarization radar. *J. Atmos. Ocean. Technol.*, **2**, 49–54.

Pielke, R. A., and M. Segal, 1986: Mesoscale circulations forced by differential terrain heating. *Mesoscale Meteorology and Forecasting*, P. Ray, Ed., *Amer. Meteor. Soc.*, 516–548.

Pratte, J. F., and R. J. Clark, 1983: PROFS mesonet—Description and performance. Preprints, *Fifth Symp. Meteorological Observation and Instrumentation*, Toronto, Amer. Meteor. Soc., 303–307.

——, J. H. VanAndel, D. G. Ferraro, R. W. Gagnon, S. M. Maher, and G. L. Blair, 1991: NCAR's mile high meteorological radar. Preprints, *25th Conf. on Radar Meteorology*, Paris, Amer. Meteor. Soc., 863–866.

Purdom, J. F. W., 1973: Satellite imagery and the mesoscale convective forecast problem. Preprints, *8th Conf. on Severe Local Storms*, Denver, Amer. Meteor. Soc., 244–251.

——, 1982: Subjective interpretations of geostationary satellite data for nowcasting. *Nowcasting*, K. Browning, Ed., Academic Press, 149–166.

Rinehart, R. E., and E. T. Garvey, 1978: Three-dimensional storm motion detection by conventional weather radar. *Nature*, **273**, 287–289.

Rogers, D., F. W. Wilson, and R. K. Goodrich, 1991: A feature identification algorithm. Preprints, *25th International Conf. on Radar Meteorology*, Paris, Amer. Meteor. Soc., 115–118.

Schaefer, J. T., 1986: The dryline. *Mesoscale Meteorology and Forecasting*, P. S. Ray, Ed., Amer. Meteor. Soc., 549–572.

Schreiber-Abshire, W., and A. R. Rodi, 1991: Mesoscale convergence zone development in northeastern Colorado under southwest flow. *Mon. Wea. Rev.*, **119**, 2956–2977.

Smolarkeiwicz, P. K., and T. L. Clark, 1985: Numerical simulation of the evolution of a three-dimensional field of cumulus clouds. Part I: Model description, comparison with observations and sensitivity studies. *J. Atmos. Sci.*, **42**, 502–522.

Szoke, E. J., M. L. Weisman, J. M. Brown, F. Caracena, and T. W. Schlatter, 1984: A sub-synoptic analysis of the Denver tornadoes of 3 June 1981. *Mon. Wea. Rev.*, **112**, 790–808.

Tsonis, A. A., and G. L. Austin, 1981: An evaluation of extrapolation techniques for the short-term prediction of rain amounts. *Atmos.-Ocean*, **19**, 54–56.

Tuttle, J. D., and G. B. Foote, 1990: Determination of the boundary layer airflow from a single Doppler radar. *J. Atmos. Oceanic. Technol.*, **7**, 218–232.

Vaughn, C. R., 1985: Birds and insects as radar targets: A review. *Proc. IEEE*, **73**, 205–227.

Westcott, N., 1984: A historical perspective on cloud mergers. *Bull. Amer. Meteor. Soc.*, **65**, 219–226.

Wilk, K. E., and K. C. Gray, 1970: Processing and analysis techniques used with the NSSL weather radar system. Preprints, *14th Conf. on Radar Meteorology*, Tucson, Amer. Meteor. Soc., 369–374.

Wilson, J. W., 1966: Movement and predictability of radar echoes. Tech. Memo, ERTM-NSSL-28, National Severe Storms Laboratory, 30 pp.

——, and R. Carbone, 1984: Nowcasting with Doppler radar: The forecaster-computer relationship. *Nowcasting II*, K. Browning, Ed., European Space Agency, 177–186.

——, and W. E. Schreiber, 1986: Initiation of convective storms by radar-observed boundary layer convergent lines. *Mon. Wea. Rev.*, **114**, 2516–2536.

——, and C. K. Mueller, 1991: Topics related to boundary layer variability and an operational experiment for 30-min forecasts of thunderstorms. Preprints, *25th Int. Conf. on Radar Meteorology*, Paris, 55–62.

——, R. E. Carbone, H. Baynton, and R. J. Serafin, 1980: Operational application of meteorological Doppler radar. *Bull. Amer. Meteor. Soc.*, **61**, 1154–1168.

——, G. B. Foote, N. A. Crook, J. C. Fankhauser, C. G. Wade, J. D. Tuttle, C. K. Mueller, S. K. Krueger, 1992: The role of boundary layer convergence zones and horizontal rolls in the initiation of thunderstorms: A case study. *Mon. Wea. Rev.*, **120**, 1785–1815.